Interconnected Pt-Nanodendrite/DNA/Reduced-Graphene-Oxide Hybrid Showing Remarkable Oxygen Reduction Activity and Stability

Jitendra N. Tiwari,[†] Kingsley Christian Kemp,[†] Krishna Nath,[‡] Rajanish N. Tiwari,[§] Hong-Gil Nam,[‡] and Kwang S. Kim[†,⊥,*]

[†]Center for Superfunctional Materials, Department of Chemistry, Pohang University of Science and Technology, San 31, Hyojadong, Namgu, Pohang 790-784, Korea, [‡]Department of New Biology, DGIST, Daegu 711-873, Korea, [§]Toyota Technological Institute, 2-12-1 Hisakata, Tampaku, Nagoya 468-8511, Japan, and [⊥]Department of Chemistry, Ulsan National Institute of Science and Technology (UNIST), UNIST-gil 50, Ulsan 689-798, Korea

ABSTRACT Controlling the morphology and size of platinum nanodendrites (PtDs) is a key factor in improving their catalytic activity and stability. Here, we report the synthesis of PtDs on genomic-double-stranded-DNA/reduced-graphene-oxide (gdsDNA/rGO) by the $NaBH_4$ reduction of H_2PtCl_6 in the presence of plant gdsDNA. Compared to industrially adopted catalysts (*i.e.*, state-of-the-art Pt/C catalyst, Pt/rGO, Pt_3Co, *etc.*), the as-synthesized PtDs/gdsDNA/rGO hybrid displays very high oxygen reduction reaction (ORR) catalytic activities (much higher than the 2015 U.S. Department of Energy (DOE) target values), which are the rate-determining steps in electrochemical energy devices, in terms of onset-potential, half-wave potential, specific-activity, mass-activity, stability, and durability. Moreover, the hybrid exhibits a highly stable mass activity for the ORR over a wide pH range of 1−13. These exceptional properties would make the hybrid applicable in next-generation electrochemical energy devices.

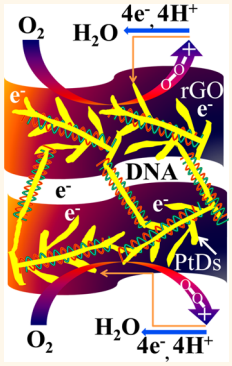

KEYWORDS: Pt nanodendrites · DNA · fuel cells · oxygen reduction reaction · catalytic activity

Platinum (Pt) metal has so far shown the greatest potential as a cathode catalyst material for the ORR in electrochemical energy devices. However, multiple problems such as kinetic limits at the cathode, crystalline facets, surface area, activity, durability, and high costs need to be solved before such devices can be commercialized for automotive, power plant, and other applications.[1−14] One method to overcome these barriers is to enhance the activity and durability of the Pt catalyst through morphology engineering using high surface area support materials. During the past decade, several methods such as high temperature alloying with other transition metals[15−18] and maximizing intrinsically more ORR active facets[19−22] have been developed to enhance the performance of Pt-based ORR catalysts. These methods have shown great improvements in ORR activity and stability; however, the lack of large-scale synthetic methods has limited their use in commercial applications. Recently, Pd−Pt bimetallic dendrites have been shown to exhibit a high ORR activity. However, these catalysts are not stable for application in commercial electrochemical energy devices with an electrochemical surface area decrease of 50% after 10000 cycles.[23] For these reasons, Pt/C catalysts still remain the most widely used in electrochemical energy devices.

Carbon allotropes and their derivatives, that is, high surface area carbon black, carbon nanotubes, highly oriented pyrolytic graphite, and reduced graphene oxide (rGO), have been studied as ORR catalyst supports.[24−27] Among these materials, the rGO is the most attractive as an ORR catalyst due to its ballistic electron conductivity, high surface area, and mechanical strength.[28−31]

Herein we describe an easy route to synthesize interconnected Pt dendrites (PtDs) on genomic-double-stranded-DNA/reduced-graphene-oxide (gdsDNA/rGO). In this process, gdsDNA is used as a template to direct the

* Address correspondence to kim@postech.ac.kr.

Received for review July 24, 2013 and accepted August 30, 2013.

Published online August 30, 2013
10.1021/nn4038404

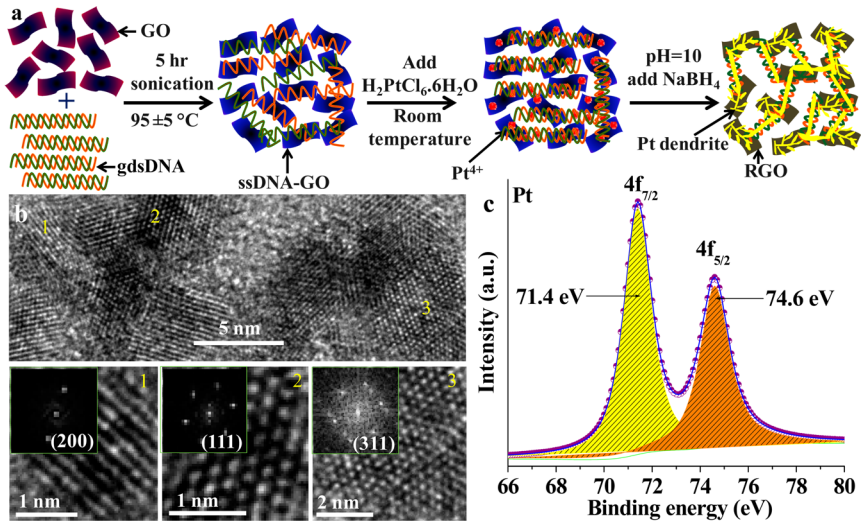

Figure 1. Synthetic procedure and their HRTEM and HRXPS analysis. (a) Schematic showing the synthetic procedure for the PtDs/gdsDNA/rGO hybrid. (b) HRTEM images of the PtDs, with branches 1−3 shown at higher magnification. Insets in parts 1−3 show the FFT patterns for the Pt branches 1−3 marked in the HRTEM. (c) Pt 4f core level HRXPS spectrum of the as-synthesized PtDs/gdsDNA/rGO hybrid.

dendritic growth of Pt by the $NaBH_4$ reduction of H_2PtCl_6. Using this simple approach, we produced a PtDs/gdsDNA/rGO hybrid with multiple active facets for the ORR in high yields. This synthesis provides an easy approach to large-scale production, as it does not require high temperatures, organic solvents, or electrochemical deposition. These PtDs formation by the reduction of Pt(IV) is contrasted with our recent work of growing very small Pt nanoclusters (~1 nm size) by the reduction of Pt(II).[6] The PtDs/gdsDNA/rGO hybrid exhibited excellent ORR activity and stability compared to the commercial state-of-the-art 20 wt % Pt/C (Pt/C; ETEK, Somerset, NJ) and Pt nanoparticles/rGO (Pt/rGO) catalysts. Importantly, the PtDs/gdsDNA/rGO hybrid displayed a constant mass activity for the ORR over a wide pH range.

RESULTS AND DISCUSSION

Our synthetic scheme for the PtDs/gdsDNA/rGO hybrid is shown in Figure 1a (for details, see Experimental Section and Supporting Information). In this synthetic method, plant gdsDNA (Supporting Information, SI, Figures S1b,c) was mixed with GO sheets (Figure S1d) and sonicated for 5 h. This dispersion was then heated at 95 ± 5 °C for 15 min. To this cooled dispersion $H_2PtCl_6 \cdot 6H_2O$ was added and the solution was incubated at room temperature for two days. Finally, a $NaBH_4$ solution was added to the dispersion and the resulting mixture was reduced at room temperature for two days. After reduction, the solution was dialyzed using a cellulose ester membrane to remove free $NaBH_4$ and Pt ions. We believe that the growth of PtDs on GO is driven by the presence of gdsDNA. The gdsDNA not only causes an accelerated $NaBH_4$ reduction of $H_2PtCl_6 \cdot H_2O$, which has been observed in other studies of the formation of nanostructures of Pt,[32−34] but also works as a driving force to position the Pt nanoparticles. Pt dendrites form as the Pt particles agglomerate in only certain orientations which depend on the surface energies of the face-centered cubic structures.

The morphologies of the Pt/rGO and PtDs/gdsDNA/rGO hybrid materials are analyzed using scanning electron microscopy (SEM; Figure S2a,b). Due to the small size of the Pt particles and PtDs in the as synthesized materials, they are further analyzed using low-resolution transmission electron microscopy (LRTEM) and high-resolution transmission electron microscopy (HRTEM). LRTEM and HRTEM images of the PtDs/gdsDNA/rGO hybrid are shown in Figures S3a,b and 1b from which we can see that the as-prepared PtDs are composed of several small Pt wire arms. In addition, the PtDs were uniformly dispersed on the rGO surface. From the HRTEM image of the single Pt branches, the fast Fourier transform (FFT) patterns (inset of Figure 1b (1−3)) were obtained, which show highly ordered continuous crystalline fringe patterns, and most of the exposed facets were found to be (311), (111), and (200). To gain insight into the surface composition of the PtDs/gdsDNA/rGO hybrid, we performed high−resolution X-ray photoelectron spectroscopy (HRXPS) analysis for the Pt 4f core-level (Figure 1c). The HRXPS Pt4f spectrum can be deconvoluted into two peaks with binding energies at 71.4 and 74.6 eV, respectively. These two peaks corresponded to the binding energies of Pt $4f_{7/2}$ and $4f_{5/2}$, which are similar to the values of metallic Pt.[35] The presence of these two peaks show that the PtDs are completely reduced using $NaBH_4$. The binding of the Pt particles to the gdsDNA in the PtDs/gdsDNA/rGO and Pt/gdsDNA catalysts is confirmed by gel electrophoresis and EDX analysis (Figure S6a,b). The structure, functional groups, elemental composition, and chemical bonding of the gdsDNA, GO, gdsDNA/GO, Pt/rGO, and PtDs/gdsDNA/rGO hybrid

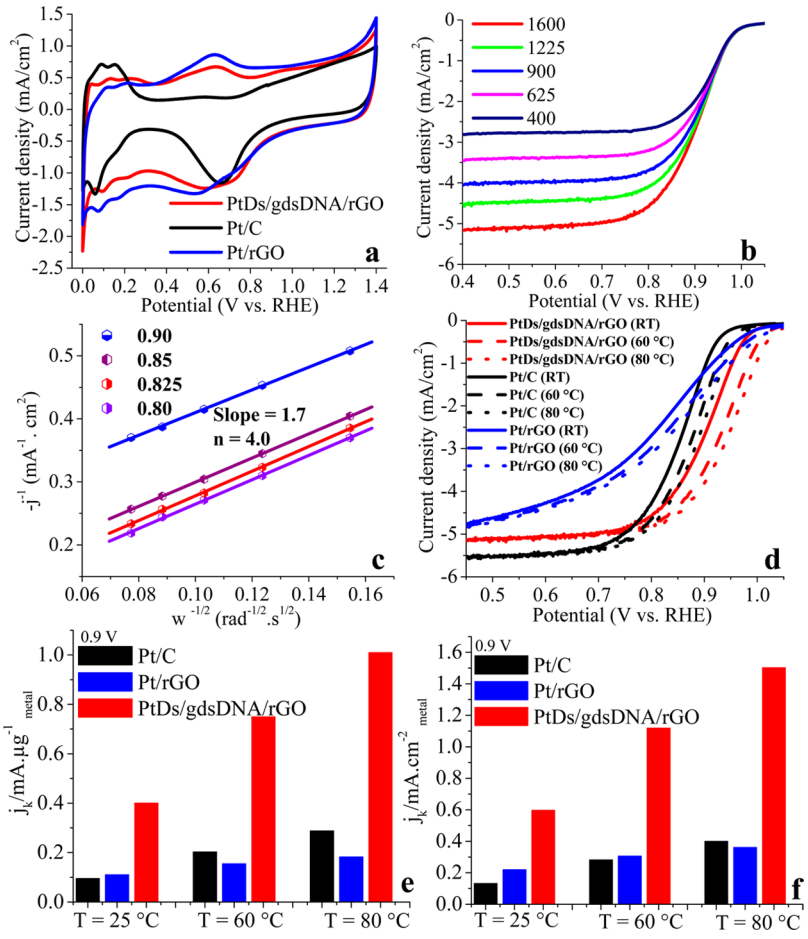

Figure 2. Electrocatalytic properties. (a) CV curves for the catalysts in N_2-saturated 0.1 M $HClO_4$ solution with a scan rate of 50 mV/s. (b) RDE curves for the PtDs/gdsDNA/rGO hybrid in O_2-saturated 0.1 M $HClO_4$ solution with a sweep rate of 10 mV/s at different rotation rates. (c) K−L plots of the PtDs/gdsDNA/rGO hybrid at various potentials. (d) RDE curves for the catalysts at 25, 60, and 80 °C in an O_2-saturated 0.1 M $HClO_4$ solution with a scan rate of 10 mV/s and a rotation speed of 1600 rpm. (e) Mass activity and (f) specific activity at 0.9 V *vs* RHE for the catalysts. Mass and specific activities are given as kinetic current densities (j_k) normalized with respect to the loading amount of Pt and EASA (EASA from CO stripping experiments), respectively. Pt loading on the RDE (geometric area = 0.0707 cm^2) for the interconnected PtDs/gdsDNA/rGO hybrid, Pt/rGO, and Pt/C catalysts was ~14.14 $\mu g/cm^2$.

materials were further analyzed using AFM, FTIR, Raman, EDX, XPS, and HRXPS to confirm that all the samples were successfully synthesized (see SI for details).

The electrochemical properties of the PtDs/gdsDNA/rGO hybrid were compared to both Pt/C (fuel cell grade) and Pt/rGO catalysts. Figure 2a shows the cyclic voltammetry (CV) curves of the catalysts in N_2-saturated 0.1 M $HClO_4$ using a glassy carbon electrode at room temperature. The CV curves display two distinctive potential regions associated with (i) the under-potential deposited hydrogen (H_{upd}) adsorption/desorption processes ($H^+ + e^- = H_{upd}$) between $0 < E < 0.37$ V and (ii) the formation of an OH_{ad} layer ($2H_2O = OH_{ad} + H_3O^+ + e^-$) beyond ~0.6 V.[23] The electrochemically active surface area (EASA) was calculated from the electric charge in the H_{upd} adsorption/desorption region, assuming that a constant 0.21 mC/cm^2 is the charge required to oxidize a monolayer of hydrogen on a smooth polycrystalline Pt surface (see SI for details). The specific EASA (EASA per unit weight of Pt) of the PtDs/gdsDNA/rGO hybrid, Pt/rGO, and Pt/C catalysts were calculated to be 57.8, 43.6, and 74.2 $m^2\ g^{-1}$, respectively. It is well-known that rGO has a very large double-layer charge, which can be clearly observed in the PtDs/gdsDNA/rGO hybrid and Pt/rGO catalyst cyclic voltammograms (Figure 2a). Due to the presence of this high double-layer capacity, the calculated EASA from the H_{upd} adsorption/desorption curve might not be very accurate. Therefore, we also carried out CO stripping CV measurements in order to obtain information on structure, and more accurate EASA of Pt catalysts. Figures S12a−c shows the CO stripping CV curves of the PtDs/gdsDNA/rGO hybrid, Pt/rGO, and Pt/C catalysts. From the charge involved in the oxidation of the adsorbed CO the EASA of the Pt/C catalyst was calculated to be 72.0 m^2/g. This value is similar to the EASA value obtained from the H_{upd} region, where the charge of desorption of a CO monolayer from a Pt surface is 420 $\mu C/cm^2$.[36−41] On the other hand, the EASA of the PtDs/gdsDNA/rGO hybrid and the Pt/rGO were calculated to be 67.2 and 50.5 m^2/g, respectively. This value is higher than that calculated from

the H_{upd} region. The larger EASA of the PtDs/gdsDNA/rGO hybrid could be attributed to the even dispersion of the PtDs on the surface of the gdsDNA/rGO hybrid. Additionally, the onset potential of CO_{ads} oxidation of the PtDs/gdsDNA/rGO hybrid (Figure S12a) is shifted by ~0.15 V toward lower potentials compared with that of the Pt/C catalyst (Figure S12c). Thus, the PtDs/gdsDNA/rGO hybrid displays an improved CO tolerance in perchloric acid electrolyte compared to the Pt/rGO and Pt/C catalysts.

Rotating-disk electrode (RDE) measurements were performed in an O_2-saturated 0.1 M $HClO_4$ solution to assess the ORR activity and kinetics of the PtDs/gdsDNA/rGO hybrid, Pt/rGO, and Pt/C catalysts. The RDE were prepared by depositing an ultrasonically dispersed aqueous catalyst onto a glassy carbon RDE at room temperature. The ORR polarization curves for the electrocatalysts are in Figures 2b,c and S13a–d. The ORR onset potentials for the PtDs/gdsDNA/rGO hybrid, Pt/rGO, and Pt/C catalysts are ~1.01, ~0.99, and ~0.95 V, respectively. Additionally, a higher ORR half-wave potential is observed for the PtDs/gdsDNA/rGO hybrid (~0.90 V) than the Pt/rGO (~0.84 V) and Pt/C (~0.85 V) catalysts.

For all the catalysts, the RDE curves in O_2-saturated 0.1 M $HClO_4$ show that the current density increases with an increase in the rotation rate from 400 to 1600 rpm (Figures 2b and S13a,c), while the corresponding Koutecky–Levich (K–L) plots display linearity (Figures 2c, and S13b,d). Linearity and parallelism in the K–L plots are indicative of first-order reaction kinetics with respect to the concentration of dissolved O_2 molecule, as well as similar electron transfer numbers for the ORR at different electrode potentials.[42] For the PtDs/gdsDNA/rGO hybrid the number of electrons transferred was calculated to be ~4.0 between 0.80–0.9 V, suggesting a four-electron pathway for the O_2 reduction process (Figure 2c). The number of electrons transferred by the Pt/C and Pt/rGO catalysts during the ORR in an O_2 saturated 0.1 M $HClO_4$ solution were 4.0 and 3.9 between 0.775–0.85 V, respectively (Figures S13b,d).

The excellent ORR activity of the PtDs/gdsDNA/rGO hybrid catalyst was also confirmed using a Tafel plot (Figure S14). The obtained Tafel slope of 60 mV/decade at a low current is very close to the value of ~63 mV/decade for the Pt/C catalyst in 0.1 M $HClO_4$. The transfer of the first electron catalyzed by PtDs/gdsDNA/rGO is probably the rate-determining step, as indicated by the Tafel slope being close to $-2.303RT/\alpha F \approx 60$ mV per decade (R, T, α, and F are the molar gas constant, absolute temperature, transfer coefficient, and Faraday constant, respectively) at room temperature.[43] From the figure it can be easily seen that the kinetic current density of PtDs/gdsDNA/rGO is far larger than that of the Pt/C catalyst in the potential region 0.8–1.0 V *versus* reversible hydrogen electrode (RHE; Figure S14).

To gain further insight into the ORR activity and kinetics of the catalysts, we performed RDE experiments at different temperatures (25, 60, and 80 °C) in an O_2 saturated 0.1 M $HClO_4$ solution at a 10 mV/s sweep rate and 1600 rpm rotation speed. The ORR polarization plots of the PtDs/gdsDNA/rGO hybrid and Pt/rGO and Pt/C catalysts are displayed in Figure 2d. The mass-transport corrected kinetic current was evaluated from the ORR polarization plots, and then this current was normalized to the loading amount of Pt in order to directly compare the mass activities of the different electrocatalysts. At 25 °C, the interconnected PtDs/gdsDNA/rGO hybrid showed a mass activity of 0.401 mA/μg_{metal} at 0.9 V *versus* RHE. This mass activity is 4.2 and 3.6 times higher than those of the Pt/C (0.0956 mA/μg_{metal}) and Pt/rGO (0.111 mA/μg_{metal}) catalysts, respectively (Figure 2e). Additionally, at 60 °C, the Pt mass activity of the PtDs/gdsDNA/rGO hybrid (0.750 mA/μg_{metal}) is higher than those of the Pt/C (0.203 mA/μg_{metal}) and Pt/rGO (0.155 mA/μg_{metal}) catalysts (Figure 2e). While at 80 °C, the PtDs/gdsDNA/rGO hybrid displayed a mass activity of 1.01 mA/μg_{metal}, which is 3.5 and 5.5 times higher than those of the Pt/C (0.288 mA/μg_{metal}, Figure 2e) and Pt/rGO (0.183 mA/μg_{metal}, Figure 2e) catalysts, respectively. Importantly, the PtDs/gdsDNA/rGO activity (1.01 mA/μg_{metal}) is much higher than the DOE target value (see Table 1) for ORR electrocatalysts (0.44 mA/μgPt at 0.9 V *vs* RHE at 80 °C) by the DOE.[44] In SI, Table S1 shows the mass activity of various ORR Pt catalysts for comparison. Therefore, the use of the PtDs/gdsDNA/rGO hybrid as an ORR catalyst is highly promising for practical applications as well as been more economically viable than currently used catalysts. Besides its excellent mass activity, we also find that the PtDs/gdsDNA/rGO hybrid displays a large specific activity. The specific activity was calculated through the normalization of the kinetic current using the catalysts EASA. At 25 °C, the interconnected PtDs/gdsDNA/rGO hybrid shows a specific activity 4.5 and 2.7 times those of the Pt/C and Pt/rGO catalysts, respectively (Figure 2f). At 60 and 80 °C the PtDs/gdsDNA/rGO hybrid showed specific activities 4.0 and 3.8 times that of the Pt/C catalyst, and 3.7 and 4.2 times higher than that of the Pt/rGO catalyst (Figure 2f). These increases in specific activity indicate accelerated ORR kinetics on the surfaces of the PtDs. The increased onset potential, half-wave potential and improved activity exhibited by the PtDs/gdsDNA/rGO hybrid could be attributed to the following factors: a) changes in morphology to facilitate fast reaction kinetics, and enhance O_2 molecular diffusion on the Pt surface and/or b) the existence of multiple ORR active (110), (111) facets along with high-index (311) facets on the Pt branches. From the CO stripping curves we can show the existence of multiple facets in the PtDs/gdsDNA/rGO hybrid by the observation of a doublet peak at 0.63 and 0.75 V *versus* RHE (Figure S11).[45–47] This is in good agreement with the TEM data, which shows multiple facets (Figure 1b). Based on previous reports, the activity of Pt toward the ORR increases with the Pt

TABLE 1. ORR Activities at 0.9 V *vs* RHE[a]

catalyst	specific activity (mA/cm^2; RT)	mass activity (mA/μg; RT)	specific activity (mA/cm^2; 60 °C)	mass activity (mA/μg; 60 °C)	specific activity (mA/cm^2; 80 °C)	mass activity (mA/μg; 80 °C)
PtDs/gdsDNA/rGO	0.597	0.401	1.120	0.750	1.503	1.010
Pt/C	0.133	0.0956	0.282	0.203	0.400	0.288
DOE target					0.720[b]	0.440[b]

[a] ORR experiments were carried out in an O_2-saturated 0.1 M $HClO_4$ solution with a scan rate of 10 mV/s and a rotation speed of 1600 rpm. [b] The 2015 stack targets at 80 °C set by the Department of Energy (DOE).

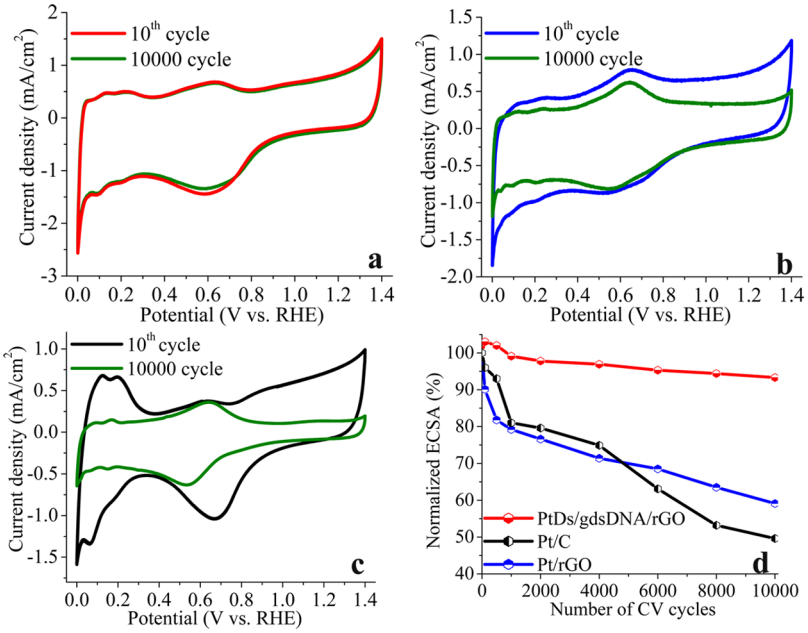

Figure 3. Electrocatalytic stability test. (a−c) CV curves for the 10th and 10000th cycles of the PtDs/gdsDNA/rGO hybrid, Pt/rGO, and Pt/C catalysts. (d) Comparison of EASA loss for the PtDs/gdsDNA/rGO hybrid, Pt/rGO and Pt/C catalysts in N_2-saturated 0.1 M $HClO_4$ solution with a cyclic potential scan between 0.0 and 1.4 V at a scan rate of 50 mV/s. Pt loading on the RDE for the interconnected PtDs/gdsDNA/rGO hybrid, Pt/rGO and Pt/C catalysts was ~14.14 μg/cm^2.

surface orientation in the order Pt(100) < Pt(111) < Pt(110).[48,49] Additionally, the gdsDNA and rGO sheets are held together by $\pi-\pi$ interactions.[50−54] The π systems show good electronic conductivity, as can be noted from graphene and π-stacked graphene systems.[55,56] Furthermore, PtDs interact with both nucleobases and the graphitic regions of rGO (due to neutral metal−π interactions[57−59]) as well as the graphene oxide regions of rGO, increasing the conductivity of the hybrid material. Thus, this increased conductivity would help easier transport of the reduced species in the gdsDNA/rGO hybrid.

Long-term stability and durability of ORR catalysts is a critical requirement for electrochemical energy devices applications. CV stability and accelerated degradation tests were carried out to examine the stability and durability of the PtDs/gdsDNA/rGO hybrid and Pt/rGO and Pt/C catalysts. Figure 3a shows the 10th and 10000th CV cycles for the PtDs/gdsDNA/rGO hybrid, from which a small degradation in performance is observed. For a clear understanding of CV stability, the normalized EASA was plotted as a function of cycle number (Figure 3d). The Pt/rGO (decreased by ~41% of the initial EASA) and Pt/C (decreased by ~51% of the initial EASA) catalysts exhibited a huge loss in EASA over 10000 cycles. In sharp contrast, a decrease in EASA (<10%) is observed for the PtDs/gdsDNA/rGO hybrid. This result clearly shows improved electrocatalytic stability for the hybrid over the Pt/rGO and Pt/C catalysts.

The durability of the catalysts was assessed using the accelerated degradation test in an O_2-saturated HClO4 solution between 0.6 and 1.2 V at a scan rate of 50 mV/s. The CV curves recorded between 0 and 1.4 V were used to calculate the EASA during potential cycling. After 10000 cycles, the Pt/rGO and Pt/C catalysts decreased by ~40 and ~41% of the initial EASA (Figures 4b and S16a,c) and showed a half wave potential degradation of ~0.07 and ~0.06 V *versus* RHE (Figure S17b,d). In contrast, the PtDs/gdsDNA/rGO hybrid showed almost no change, with only ~7% loss in initial Pt EASA (Figure 4a,b) and no significant decrease (less than ~0.01 V) in a half wave potential decrease *versus* RHE (Figure 4c). These results show that the PtDs/gdsDNA/rGO hybrid displays an excellent

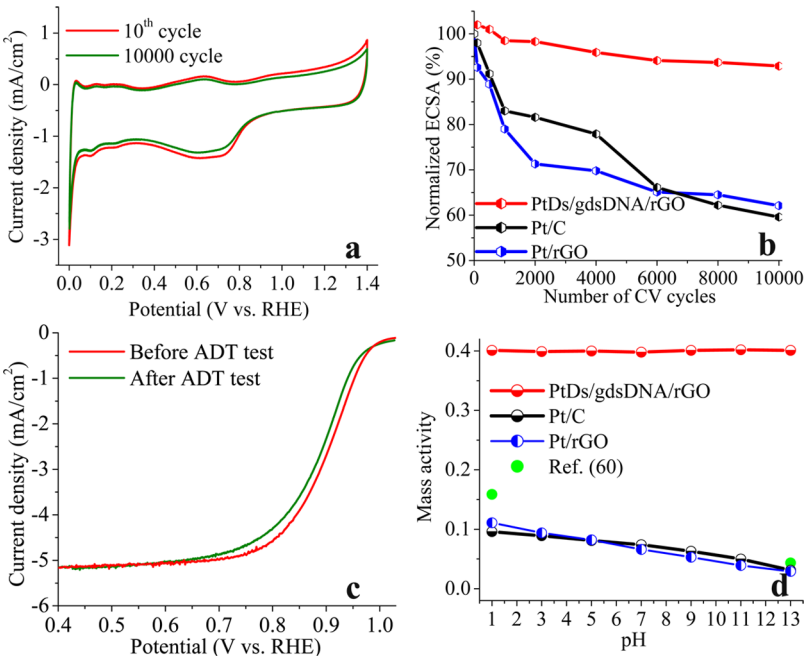

Figure 4. Electrocatalytic durability and pH dependent mass activity test. (a) CV curves for the 10th and 10000th cycles of the PtDs/gdsDNA/rGO hybrid. (b) Comparison of EASA loss for the PtDs/gdsDNA/rGO hybrid, Pt/rGO, and Pt/C catalysts in O_2-saturated 0.1 M $HClO_4$ solution with a cyclic potential scan between 0.6 and 1.2 V at a scan rate of 50 mV/s. (c) Polarization curves for the PtDs/gdsDNA/rGO hybrid samples before and after the accelerated durability test (ADT). (d) The mass activity of the catalysts was estimated in O_2-saturated solutions of various pH, with scan rate 10 mV/s and rotation speed 1600 rpm. The mass activity values are an average calculated from five independent experiments. Pt loading on the RDE for the interconnected PtDs/gdsDNA/rGO hybrid, Pt/rGO, and Pt/C catalysts was ~14.14 μg/cm^2.

durability performance compared to that of the Pt/C and Pt/rGO catalysts. To further examine the catalysts durability their structures were observed after cycling by using LRTEM and HRTEM. After the accelerated degradation test, the catalysts were collected by sonicating the glassy carbon electrode (GCE) in ethanol. Figures S17 and S18 show the TEM images of the Pt/rGO, Pt/C and PtDs/gdsDNA/rGO catalysts. For the Pt/rGO catalyst, there is an increase in Pt nanoparticle size from ~3 to ~20 nm (Figure S17c), while the Pt/C catalyst shows an increase of ~3 to ~10 nm (Figure S17d). This increase in Pt nanoparticle is due to Ostwald ripening and aggregation, and additionally an uneven dispersion and detachment of Pt nanoparticles is observed due to degradation of the carbon or rGO supports (Figure S17c,d). On the other hand, for the PtDs/gdsDNA/rGO hybrid, the PtDs are well-dispersed on the gdsDNA/rGO, and their sizes are only slightly increased (Figure S18a). This demonstrates that plant gdsDNA provides a surface stability for the PtDs, as is evident from the clearly visualized lattice spacings (Figure S18b–d). This increased ORR stability arises from higher stability of PtDs over Pt nanoparticles, as well as morphological stabilization of the hybrids by DNA linkages between the rGO sheets.

Finally, the ORR activity for the catalysts over a wide pH range was determined (Figure 4d). The PtDs/gdsDNA/rGO hybrid exhibited a uniform mass activity (0.401) over the pH range of 1–13, whereas the ORR mass activities of Pt/C, Pt/rGO, and 46 wt % Pt/C[60] catalysts vary as the pH changed. The remarkable pH stability of the interconnected PtDs/gdsDNA/rGO hybrid could be ascribed to the $\pi-\pi$ interactions between rGO sheets and gdsDNA side chains as well as the neural metal–π interactions of PtDs with both gdsDNA and rGO. The $\pi-\pi$ stacking (hydrophobic interactions between the nucleobases of the gdsDNA and the graphitic domains of rGO sheets)[50−54] are hardly affected by acids and bases involving proton transfer induced electrostatic interactions, which helps corrosion-resistance. Furthermore, PtDs interact with both the nucleobases of gdsDNA and the graphitic regions of rGO.[57−59] These neural metal–π interactions are also little affected by the acids and bases because neutral PtDs are safe to a certain extent over the electrostatic environmental changes under proton exchanges, which results in corrosion-resistance; otherwise, the PtDs could aggregate together, which could result in degradation of the catalytic activity. Although PtDs interact with both phosphate groups of the gdsDNA graphene oxide regions of rGO, which would be susceptible for acids and bases environments, this hybrid material could be well sustained because of the above neural metal–π interactions along with the $\pi-\pi$ interactions.

CONCLUSIONS

In summary, we have synthesized the interconnected PtDs on gdsDNA/rGO. Compared to industrially adopted catalysts (*i.e.*, state-of-the-art Pt/C catalyst,

Pt/G, Pt_3Co, *etc.*), the as-synthesized PtDs/gdsDNA/rGO hybrid shows an outstanding catalytic activity toward ORR, with respect to onset potential, half-wave potential, mass activity, specific activity, stability, and durability. Moreover, the PtDs/gdsDNA/rGO hybrid exhibited a constant mass activity for the ORR over a wide pH range (pH = 1−13). Given that the ORR catalytic activity has been the rate-determining step in electrochemical energy devices, all those exceptional properties make us believe that PtDs/gdsDNA/rGO hybrid can be utilized in next generation electrochemical energy devices.

EXPERIMENTAL SECTION

Preparation of the PtDs/gdsDNA/rGO Hybrid and Pt/rGO Catalyst. The details of preparation processes for gdsDNA, GO and gdsDNA/GO are given in the SI. The synthesis of the 20 wt % PtDs/gdsDNA/rGO hybrid was achieved by mixing 106 mg of $H_2PtCl_6 \cdot 6H_2O$ (ACS reagent, ≥37.50% Pt basis) with 54 mL of a gdsDNA/rGO suspension followed by incubation at room temperature for two days with vigorous stirring. To this mixture a 50 mL sodium borohydride solution (5 mg/mL) was added and the reaction mixture was allowed to reduce at room temperature for two days with continuous stirring. The resulting solution was purified by dialysis through cellulose membranes to remove free Pt ions and sodium borohydride. For the synthesis of the 20 wt % Pt nanoparticles/rGO (Pt/rGO), the same procedure was followed, with a GO dispersion instead of a gdsDNA/rGO suspension.

Physical and Chemical Characterization. The DNA sample was prepared by dropping an extracted gdsDNA solution onto to a Si surface. Atomic force microscopy (AFM) images were recorded using an AFM, Bruker-N8 NEOS. Fourier transform infrared (FTIR) spectra were recorded in KBr pellets using a Bruker FTIR. Measurements of micro Raman spectra were carried out using a Senterra Raman Scope system with a 532 nm wavelength incident laser light and power 20 mW. The morphologies of the synthesized materials were characterized using a field-emission SEM (FESEM, JEOL, FEG-XL 30S) with an acceleration voltage of 5 kV. TEM and HRTEM observations were carried out using a JEM-2200FS (Cs-corrected STEM) electron microscope with an accelerating voltage of 200 kV. The HRXPS analysis was performed with an ESCALAB-220I-XL (Thermo-Electron, VG Company) system.

Electrocatalytic Measurements. All electrocatalytic experiments were performed using a glassy carbon RDE (Bio-Logic Science Instruments) connected to a VSP-Modular 2 Channels Potentiostat/Galvanostat/EIS. A three-electrode-system consisting of a modified GCE (3 mm in diameter) as the working electrode, Ag/AgCl (3 M NaCl) as the reference electrode, and a Pt wire as the counter electrode was used. All potentials were converted to values with reference to RHE. In order to perform the RHE conversion, the thermodynamic potential for the hydrogen electrode was obtained using cyclic voltammetry. From cyclic sweeps at a rate of 1 mV/s, the average of the two potentials at which the current crosses zero was taken to be the thermodynamic potential for the hydrogen electrode reaction. All reagents were of analytical grade and were used without further purification. Deionized (DI) water was used to prepare all solutions. The electrolyte was 0.1 M $HClO_4$ aqueous diluted from 70% $HClO_4$ (Baker, ACS Reagent grade) using DI water. pH curves were obtained by measuring the catalysts ORR mass activity in O_2-saturated solutions at various pH. The pH was adjusted by adding the required amount of either $HClO_4$ or NaOH during the preparation of the solutions.

Further details for the sample synthesis, preparation, and electrochemical measurements can be found in the SI.

Conflict of Interest: The authors declare no competing financial interest.

Acknowledgment. This work was supported by NRF (National Honor Scientist Program: 2010-0020414). The work of H.G.N. was supported by a grant from the NRF through the National Research Support Program (No. 2010-0020417). Dr. Nam-Suk Lee is acknowledged for measurement of HRTEM, which was done in the National Center for Nanomaterials Technology (NCNT) at POSTECH, Korea.

Supporting Information Available: Experimental procedures and Figures S1−S18 and Tables S1−S2. This material is available free of charge *via* the Internet at http://pubs.acs.org.

REFERENCES AND NOTES

1. Debe, M. K. Electrocatalyst Approaches and Challenges for Automotive Fuel Cells. *Nature* **2012**, *486*, 43–51.
2. Tiwari, J. N.; Tiwari, R. N.; Singh, G.; Kim, K. S. Recent Progress in the Development of Anode and Cathode Catalysts for Direct Methanol Fuel Cells. *Nano Energy* **2013**, *2*, 553–578.
3. Tiwari, J. N.; Tiwari, R. N.; Kim, K. S. Zero-Dimensional, One-Dimensional, Two-Dimensional, and Three-Dimensional Nanostructured Materials for Advanced Electrochemical Energy Devices. *Prog. Mater. Sci.* **2012**, *57*, 724–803.
4. Mallouk, T. E. Fuel Cells: Miniaturized Electrochemistry. *Nature* **1990**, *343*, 515–516.
5. Steele, B. C. H.; Heinzel, A. Materials for Fuel-Cell Technologies. *Nature* **2001**, *414*, 345–352.
6. Tiwari, J. N.; Nath, K.; Kumar, S.; Tiwari, R. N.; Kemp, K. C.; Le, N. H.; Youn, D. H.; Lee, J. S.; Kim, K. S. Stable Platinum Nanoclusters on Genomic DNA−Graphene Oxide with a High Oxygen Reduction Reaction Activity. *Nat. Commun.* **2013**, *4*, 2221.
7. Yamamoto, K.; Imaoka, T.; Chun, W. J.; Enoki, O.; Katoh, H.; Takenaga, M.; Sonoi, A. Size-Specific Catalytic Activity of Platinum Clusters Enhances Oxygen Reduction Reactions. *Nat. Chem.* **2009**, *1*, 397–402.
8. Greeley, J.; Stephens, I. E. L.; Bondarenko, A. S.; Johansson, T. P.; Hansen, H. A.; Jaramillo, T. F.; Rossmeisl, J.; Chorkendorff, I.; Nørskov, J. K. Alloys of Platinum and Early Transition Metals as Oxygen Reduction Electrocatalysts. *Nat. Chem.* **2009**, *1*, 552–556.
9. Wang, C.; Daimon, H.; Lee, Y.; Kim, J.; Sun, S. Synthesis of Monodisperse Pt Nanocubes and Their Enhanced Catalysis for Oxygen Reduction. *J. Am. Chem. Soc.* **2007**, *129*, 6974–6975.
10. Xia, B. Y.; Ng, W. T.; Wu, H. B.; Wang, X.; Lou, X. W. Self-Supported Interconnected Pt Nanoassemblies as Highly Stable Electrocatalysts for Low-Temperature Fuel Cells. *Angew. Chem., Int. Ed.* **2012**, *51*, 1–5.
11. Sun, S.; Zhang, G.; Geng, D.; Chen, Y.; Li, R.; Cai, M.; Sun, X. A Highly Durable Platinum Nanocatalyst for Proton Exchange Membrane Fuel Cells: Multiarmed Starlike Nanowire Single Crystal. *Angew. Chem., Int. Ed.* **2011**, *50*, 422–426.
12. Kibsgaard, J.; Gorlin, Y.; Chen, Z.; Jaramillo, T. F. Meso-Structured Platinum Thin Films: Active and Stable Electrocatalysts for the Oxygen Reduction Reaction. *J. Am. Chem. Soc.* **2012**, *134*, 7758–7765.
13. Li, Y.; Li, Y.; Zhu, E.; McLouth, T.; Chiu, C.-Y.; Huang, X.; Huang, Y. Stabilization of High-Performance Oxygen Reduction Reaction Pt Electrocatalyst Supported on Reduced Graphene Oxide/Carbon Black Composite. *J. Am. Chem. Soc.* **2012**, *134*, 12326–12329.
14. Koenigsmann, C.; Sutter, E.; Chiesa, T. A.; Adzic, R. R.; Wong, S. S. Highly Enhanced Electrocatalytic Oxygen Reduction Performance Observed in Bimetallic Palladium-Based Nanowires Prepared Under Ambient, Surfactantless Conditions. *Nano Lett.* **2012**, *12*, 2013–2020.
15. Mukerjee, S.; Srinivasan, S. Enhanced Electrocatalysis of Oxygen Reduction on Platinum Alloys in Proton Exchange Membrane Fuel Cells. *J. Electroanal. Chem.* **1993**, *357*, 201–224.

16. Mukerjee, S.; Srinivasan, S.; Soriaga, M. P.; McBreen, J. Role of Structural and Electronic Properties of Pt and Pt Alloys on Electrocatalysis of Oxygen Reduction an *In Situ* XANES and EXAFS Investigation. *J. Electrochem. Soc.* **1995**, *142*, 1409–1422.
17. Vayssilov, G. N.; Lykhach, Y.; Migani, A.; Staudt, T.; Petrova, G. P.; Tsud, N.; Skála, T.; Bruix, A.; Illas, F.; Prince, K. C.; *et al*. Support Nanostructure Boosts Oxygen Transfer to Catalytically Active Platinum Nanoparticles. *Nat. Mater.* **2011**, *10*, 310–315.
18. Wu, G.; More, K. L.; Johnston, C. M.; Zelenay, P. High-Performance Electrocatalysts for Oxygen Reduction Derived from Polyaniline, Iron, and Cobalt. *Science* **2011**, *332*, 443–447.
19. Narayanan, R.; El-Sayed, M. A. Shape-Dependent Catalytic Activity of Platinum Nanoparticles in Colloidal Solution. *Nano Lett.* **2004**, *4*, 1343–1348.
20. Tian, N.; Zhou, Z.-Y.; Sun, S.-G.; Ding, Y.; Wang, Z. L. Synthesis of Tetrahexahedral Platinum Nanocrystals with High-Index Facets and High Electro-Oxidation Activity. *Science* **2007**, *316*, 732–735.
21. Bratlie, K. M.; Lee, H.; Komvopoulos, K.; Yang, P.; Somorjai, G. A. Platinum Nanoparticle Shape Effects on Benzene Hydrogenation Selectivity. *Nano Lett.* **2007**, *7*, 3097–3101.
22. Wang, C.; Daimon, H.; Onodera, T.; Koda, T.; Sun, S. A General Approach to the Size- and Shape-Controlled Synthesis of Platinum Nanoparticles and Their Catalytic Reduction of Oxygen. *Angew. Chem., Int. Ed.* **2008**, *47*, 3588–3591.
23. Lim, B.; Jiang, M.; Camargo, P. H. C.; Cho, E. C.; Tao, J.; Lu, X.; Zhu, Y.; Xia, Y. Pd-Pt Bimetallic Nanodendrites with High Activity for Oxygen Reduction. *Science* **2009**, *324*, 1302–1305.
24. Wu, J.; Zhang, J.; Peng, Z.; Yang, S.; Wagner, F. T.; Yang, H. Truncated Octahedral Pt_3Ni Oxygen Reduction Reaction Electrocatalysts. *J. Am. Chem. Soc.* **2010**, *132*, 4984–4985.
25. Li, W.; Liang, C.; Zhou, W.; Qiu, J.; Zhou, Z.; Sun, G.; Xin, Q. Preparation and Characterization of Multiwalled Carbon Nanotube-Supported Platinum for Cathode Catalysts of Direct Methanol Fuel Cells. *J. Phys. Chem. B* **2003**, *107*, 6292–6299.
26. Tiwari, J. N.; Tiwari, R. N.; Chang, Y. M.; Lin, K. L. A Promising Approach to the Synthesis of 3D Nanoporous Graphitic Carbon as a Unique Electrocatalyst Support for Methanol Oxidation. *ChemSusChem* **2010**, *3*, 460–466.
27. Zhou, Y.; Pasquarelli, R.; Holme, T.; Berry, J.; Ginley, D.; O'Hayre, R. Improving PEM Fuel Cell Catalyst Activity and Durability Using Nitrogen-Doped Carbon Supports: Observations from Model Pt/HOPG Systems. *J. Mater. Chem.* **2009**, *19*, 7830–7838.
28. Georgakilas, V.; Otyepka, M.; Bourlinos, A. B.; Chandra, V.; Kim, N.; Kemp, K. C.; Hobza, P.; Zboril, R.; Kim, K. S. Functionalization of Graphene: Covalent and Non-Covalent Approaches, Derivatives, and Applications. *Chem. Rev.* **2012**, *112*, 6156–6214.
29. Stankovich, S.; Dikin, D. A.; Dommett, G. H. B.; Kohlhaas, K. M.; Zimney, E. J.; Stach, E. A.; Piner, R. D.; Nguyen, S. T.; Ruoff, R. S. Graphene-Based Composite Materials. *Nature* **2006**, *442*, 282–286.
30. Park, S.; Ruoff, R. S. Chemical Methods for the Production of Graphenes. *Nat. Nanotechnol.* **2009**, *4*, 217–224.
31. Kim, D. S.; Kim, C.; Kim, J. K.; Kim, J. H.; Chun, H. H.; Lee, H.; Kim, Y. T. Enhanced Electrocatalytic Performance due to Anomalous Compressive Strain and Superior Electron Retention Properties of Highly Porous Pt Nanoparticles. *J. Catal.* **2012**, *291*, 69–75.
32. Song, Y.; Yang, Y.; Medforth, C. J.; Pereira, E.; Singh, A. K.; Xu, H.; Jiang, Y.; Brinker, C. J.; Swol, F.; Shelnutt, J. A. Controlled Synthesis of 2-D and 3-D Dendritic Platinum Nanostructures. *J. Am. Chem. Soc.* **2004**, *126*, 635–645.
33. Chen, J.; Herricks, T.; Xia, Y. Polyol Synthesis of Platinum Nanostructures: Control of Morphology Through the Manipulation of Reduction Kinetics. *Angew. Chem., Int. Ed.* **2005**, *44*, 2589–2592.
34. Lim, B.; Lu, X.; Jiang, M.; Camargo, P. H. C.; Cho, E. C.; Lee, E. P.; Xia, Y. Facile Synthesis of Highly Faceted Multioctahedral Pt Nanocrystals Through Controlled Overgrowth. *Nano Lett.* **2008**, *8*, 4043–4047.
35. Xin, Y. C.; Liu, J. G.; Zhou, Y.; Liu, W. M.; Gao, J. A.; Xie, Y.; Yin, Y.; Zou, Z. G. Preparation and Characterization of Pt Supported on Graphene with Enhanced Electrocatalytic Activity in Fuel Cell. *J. Power Sources* **2011**, *196*, 1012–1018.
36. Tiwari, J. N.; Tiwari, R. N.; Lin, K.-L. Synthesis of Pt Nanopetals on Highly Ordered Silicon Nanocones for Enhanced Methanol Electrooxidation Activity. *ACS Appl. Mater. Interfaces* **2010**, *2*, 2231–2237.
37. Gasteiger, H. A.; Marković, N.; Ross, P. N.; Cairns, E. J. Carbon Monoxide Electrooxidation on Well-Characterized Platinum-Ruthenium Alloys. *J. Phys. Chem.* **1994**, *98*, 617–625.
38. Tiwari, J. N.; Pan, F.-M.; Chen, T.-M.; Tiwari, R. N.; Lin, K.-L. Electrocatalytic Activity of Pt Nanoparticles Electrodeposited on Amorphous Carbon-Coated Silicon Nanocones. *J. Power Sources* **2010**, *195*, 729–735.
39. Tiwari, J. N.; Pan, F.-M.; Lin, K.-L. Facile Approach to the Synthesis of 3D Platinum Nanoflowers and Their Electrochemical Characteristics. *New J. Chem.* **2009**, *33*, 1482–1485.
40. Tiwari, J. N.; Pan, F.-M.; Tiwari, R. N.; Nandi, S. K. Facile Synthesis of Continuous Pt Island Networks and Their Electrochemical Properties for Methanol Electrooxidation. *Chem. Commun.* **2008**, *48*, 6516–6518.
41. Tiwari, J. N.; Chen, T.-M.; Pan, F.-M.; Lin, K.-L. Ordered Silicon Nanocones as a Highly Efficient Platinum Catalyst Support for Direct Methanol Fuel Cells. *J. Power Sources* **2008**, *182*, 510–514.
42. Liang, Y. Y.; Li, Y. G.; Wang, H. G.; Zhou, J. G.; Wang, J. J.; Regier, T.; Dai, H. J. Co_3O_4 Nanocrystals on Graphene as a Synergistic Catalyst for Oxygen Reduction Reaction. *Nat. Mater.* **2011**, *10*, 780–786.
43. Anderson, A. B.; Sidik, R. A. Oxygen Electroreduction on Fe^{II} and Fe^{III} Coordinated to N_4 Chelates. Reversible Potentials for the Intermediate Steps from Quantum Theory. *J. Phys. Chem. B* **2004**, *108*, 5031–5035.
44. Gasteiger, H. A.; Kocha, S. S.; Sompalli, B.; Wagner, F. T. Activity Benchmarks and Requirements for Pt, Pt-Alloy, and Non-Pt Oxygen Reduction Catalysts for PEMFCs. *Appl. Catal., B* **2005**, *56*, 9–35.
45. Bergelin, M.; Feliu, J. M.; Wasberg, M. Study of Carbon Monoxide Adsorption and Oxidation on Pt(111) by Using an Electrochemical Impinging Jet Cell. *Electrochim. Acta* **1997**, *44*, 1069–1075.
46. Hayden, B. E.; Murray, A. J.; Parsons, R.; Pegg, D. J. UHV and Electrochemical Transfer Studies on Pt(110)-(1 × 2): The Influence of Bismuth on Hydrogen and Oxygen Adsorption, and the Electro-Oxidation of Carbon Monoxide. *J. Electroanal. Chem.* **1996**, *409*, 51–63.
47. Koponen, U.; Peltonen, T.; Bergelin, M.; Mennola, T.; Valkiainen, M.; Kaskimies, J.; Wasberg, M. The Impinging Jet Flow Cell-a Novel Method for the Study of PEM Fuel Cell Material. *J. Power Sources* **2000**, *86*, 261–268.
48. Stamenkovic, V. R.; Fowler, B.; Mun, B. S.; Wang, G.; Ross, P. N.; Lucas, C. A.; Marković, N. M. Improved Oxygen Reduction Activity on $Pt_3Ni(111)$ *via* Increased Surface Site Availability. *Science* **2007**, *315*, 493–497.
49. Koenigsmann, C.; Scofield, M. E.; Liu, H. Q.; Wong, S. S. Designing Enhanced One-Dimensional Electrocatalysts for the Oxygen Reduction Reaction: Probing Size- and Composition-Dependent Electrocatalytic Behavior in Noble Metal Nanowires. *J. Phys. Chem. Lett.* **2012**, *3*, 3385–3398.
50. Patil, A. J.; Vickery, J. L.; Scott, T. B.; Mann, S. Aqueous Stabilization and Self-Assembly of Graphene Sheets into Layered Bio-Nanocomposites Using DNA. *Adv. Mater.* **2009**, *21*, 3159.
51. Xu, Y. X.; Wu, Q.; Sun, Y. Q.; Bai, H.; Shi, G. Q. Three-Dimensional Self-Assembly of Graphene Oxide and DNA into Multifunctional Hydrogels. *ACS Nano* **2010**, *4*, 7358–7362.
52. Cho, Y.; Min, S. K.; Yun, J.; Kim, W. Y.; Tkatchenko, A.; Kim, K. S. Noncovalent Interactions of DNA Bases with Naphthalene and Graphene. *J. Chem. Theory Comput.* **2013**, *9*, 2090–2096.
53. Min, S. K.; Kim, W. Y.; Cho, Y.; Kim, K. S. Fast DNA Sequencing with a Graphene-Based Nanochannel Device. *Nat. Nanotechnol.* **2011**, *6*, 162–165.

54. Kim, K. S.; Tarakeshwar, P.; Lee, J. Y. Molecular Clusters of π-Systems: Theoretical Studies of Structures, Spectra, and Origin of Interaction Energies. *Chem. Rev.* **2000**, *100*, 4145–4186.
55. Kim, K. S.; Zhao, Y.; Jang, H.; Lee, S. Y.; Kim, J. M.; Kim, K. S.; Ahn, J.-H.; Kim, P.; Choi, J.-Y.; Hong, B. H. Large-Scale Pattern Growth of Graphene Films for Stretchable Transparent Electrodes. *Nature* **2009**, *457*, 706–710.
56. Lee, W. H.; Park, J.; Sim, S. H.; Jo, S. B.; Kim, K. S.; Hong, B. H.; Cho, K. Transparent Flexible Organic Transistors Based on Monolayer Graphene Electrodes on Plastic. *Adv. Mater.* **2011**, *23*, 1752–1756.
57. Yi, H.-B.; Diefenbach, M.; Choi, Y. C.; Lee, E. C.; Lee, H. M.; Hong, B. H.; Kim, K. S. Interactions of Neutral and Cationic Transition Metals with the Redox System of Hydroquinone and Quinone: Theoretical Characterization of the Binding Topologies, and Implications for the Formation of Nanomaterials. *Chem.—Eur. J.* **2006**, *12*, 4885–4892.
58. Yi, H.-B.; Lee, H. M.; Kim, K. S. Interaction of Benzene with Transition Metal Cations: Theoretical Study of Structures, Energies, and IR Spectra. *J. Chem. Theory Comput.* **2009**, *5*, 1709–1717.
59. Youn, I. S.; Kim, D. Y.; Singh, N. J.; Park, S. W.; Youn, J.; Kim, K. S. Intercalation of Transition Metals into Stacked Benzene Rings: A Model Study of the Intercalation of Transition Metals into Bi-Layered Graphene. *J. Chem. Theory Comput.* **2012**, *8*, 99–105.
60. Meng, H.; Jaouen, F.; Proietti, E.; Lefevre, M.; Dodelet, J.-P. pH-Effect on Oxygen Reduction Activity of Fe-Based Electro-Catalysts. *Electrochem. Commun.* **2009**, *11*, 1986–1989.